

Propagation and Diffraction of Picosecond Acoustic Wave Packets in the Soliton Regime

Otto L. Muskens and Jaap I. Dijkhuis

Atom Optics and Ultrafast Dynamics, Debye Institute, University of Utrecht,
P.O. Box 80 000, 3508 TA, Utrecht, Netherlands

Abstract. Recent experiments on propagation of picosecond acoustic wave packets in condensed matter have opened up a new, exciting area of soliton physics. Single cycle strain pulses as short as several picoseconds can be generated in a thin metallic film, yielding local strain fields of the order of 10^{-4} . The combination of phonon dispersion and anharmonicity of the atomic interaction potential may give rise to strongly nonlinear, but stable propagation of the wave packets over a distance of the order of several millimeters in a single crystalline material. We present new results on nonlinear propagation of acoustic wave packets created by nJ femtosecond optical pulses in a lead molybdate single crystal, employing the Brillouin scattering technique as a local probe of acoustic strain. Studies of diffraction of narrow discs of acoustic strain show anomalous diffraction of the various Fourier components constituting the wave packet. Propagation of virtually one-dimensional nature is studied by exciting the metal film over a large area using an amplified femtosecond laser. We show that these data can be interpreted by means of the Korteweg-de Vries equation and strongly suggest the development of acoustic solitons.

1 Introduction

The discovery of nonlinear optical phenomena in various areas of experimental condensed matter physics has led to a multitude of potential technological applications. In comparison with the field of nonlinear optics, nonlinear wave phenomena in acoustics have received remarkably little attention. Only recently, acoustic solitons, an archetypical nonlinear wave phenomenon, have been generated in an elastic rod [1], using an exploding metallic flyer foil in water as the generator of high acoustic strain. Here, unipolar (compressional) acoustic strain fields were produced of several microseconds duration. To observe soliton development, a very substantial degree of anomalous dispersion is required. This dispersion was provided in the rod by the modes of an acoustic waveguide.

A completely different regime for stable soliton formation has been explored by Hao and Maris [2][3]. It was already predicted by Breazale and Ford [4] that, given the weak anharmonicity of a realistic solid, for a piezoelectrically generated ultrasonic wave in the MHz regime a discontinuity - or shock wave, another prototype nonlinearity - would only develop after a travelled distance

of, say, 500 cm. This explains why in ultrasound experiments in crystalline solids nonlinear acoustical phenomena have remained a relatively unexplored field for a long time. The situation changes dramatically if one replaces the MHz strain field by a wave packet containing much higher frequency components, say, of the order of tens of GHz, as can be generated using high intensity, ultrashort optical excitation in a thin metal transducer [2][3][5]. Under these conditions the discontinuity distance drops to the order of a few millimeters and experiments are well within reach. A fortitious circumstance is the fact that the metal film is not necessarily destroyed or modified in the optical experiments, which enables doing repetitive experiments. The acoustic strain generated by the method of pulsed optical excitation in a metal film in general is bipolar, therefore both anomalous and normal dispersion may lead to acoustic soliton formation for either polarities. It turns out that the normal phonon dispersion of longitudinal acoustic lattice modes in crystals in combination with the lattice anharmonicity can be sufficient to develop stable propagating solitons [2]. In general, experiments at these high acoustic frequencies require working at liquid helium temperatures, in order to reduce thermal damping of these acoustic fields, that otherwise prevents the buildup of solitary waves.

The most striking difference between picosecond acoustic wave packets and those studied in nonlinear optics is the fact that the initial excitation is a *single cycle* wave packet, rather than an slowly varying modulation of the carrier frequency. This makes the acoustic system a very interesting and new system to study one- and higher-dimensional propagation effects in detail. As the disturbance is propagating with the velocity of sound and can be easily detected by optical means, it is a much more accessible subject to study than an optical disturbance. In particular, it is feasible to obtain information both on the amplitude and the phase of the strain field by means of time domain interferometry (see e.g. Hurley and Wright [6]).

2 Theory

In the following we will briefly introduce the ideas and concepts of nonlinear acoustics. A finite local distortion of an anisotropic lattice $\mathbf{u}(\mathbf{r}, t)$ generates a deformation Δ , which is usually defined in terms of the acoustic strain tensor $\eta(\mathbf{r}, t)$, by [7]

$$\begin{aligned} \Delta &= \eta_{ij} dr_i dr_j \\ \eta_{ij} &= \frac{1}{2} (q_{ij} + q_{ji} + q_{ik}q_{kj}) , \end{aligned} \quad (1)$$

where

$$q_{ij} = \frac{\partial u_i}{\partial r_j} \quad (2)$$

describes the displacement gradient matrix elements. To obtain the correct nonlinear elastic wave equations, one has to take into account this complete expression for the strain tensor, including the last term on the right hand side (which

is neglected in linear elasticity theory). The generated strain yields a stress T in the crystal via the interparticle interactions. This can be found in terms of the derivative of the lattice free energy ϕ to the Lagrangian coordinates q_{ij} [8]

$$T_{ij} = \frac{\partial \phi}{\partial q_{ij}} . \quad (3)$$

The equation of motion for finite strains can then in turn be formulated in terms of this stress tensor and the mass density ρ

$$\rho \mathbf{u}_{tt} = \nabla \cdot T , \quad (4)$$

where the subscript denotes the partial time derivative. It has been shown that for adiabatic deformation, the internal energy ϕ can be expressed as a power series of the first three invariants of the strain tensor, in combination with the appropriate elastic constants of second and third order [8][9]. For isotropic solids there are five of these elastic moduli (the so called 'five-constant' theory, see e.g. Ref. [10]). Expressions for several crystal groups of high symmetry have also been found by Seeger and Buck [9]. For these expressions for the internal energy (consisting of 36 terms for the cubic symmetry group) we refer to literature. In the case of one-dimensional propagation along an axis of high symmetry, the equation of motion however reduces to the simple form [4]

$$\rho u_{tt} = \gamma u_{zz} + \alpha u_z u_{zz} . \quad (5)$$

The last term on the right side is the quadratic nonlinearity, due to the geometric nonlinearity of (1) and the cubic terms in the inter-atomic potential. The nonlinearity coefficient α depends only on the propagation direction in the crystal [11]. For the [001] direction in a cubic crystal the two constants of (5) take on the form [4]

$$\begin{aligned} \gamma &= C_{33} \\ \alpha &= (3C_{33} + C_{333}) , \end{aligned} \quad (6)$$

where the coefficients C_{33} and C_{333} are the second- and third-order elastic moduli in the [001] direction. For most solids, the contribution of the third order modulus is larger than the geometric term and has a negative sign, yielding an $\alpha < 0$.

Up to this point we have not taken into account any dispersion in the equation of motion. In the case of longitudinal acoustic lattice vibrations (LA phonons) in a crystalline solid, the dispersion due to discreteness of the lattice can be written as

$$\omega = \sqrt{\frac{4C_{33}}{M}} \sin |ka/2| . \quad (7)$$

As we will be dealing with vibrations of small wavevector, i.e. in the center of the Brillouin zone, it is sufficient to approximate this dispersion relation by its first two nonzero expansion terms

$$\begin{aligned} \omega &= v_0 k - \beta k^3 , \\ \beta &= \frac{v_0^3}{6\omega_{max}^2} , \end{aligned} \quad (8)$$

where ω_{max} is the LA angular frequency at the edge of the Brillouin zone. This dispersive correction can be put into (5), leading to a fourth order spatial derivative (see e.g. Hao and Maris [2]). At this point it is further convenient to switch from the displacement coordinate u to the z -component of the acoustic strain η . This is done by differentiation of (5) with respect to the z -coordinate. Given the initial wave packet at $t = 0$ of amplitude η_0 and shape $\psi(z)$, the resulting boundary value problem including dispersion, reads

$$\eta_{tt} - c_0^2 \eta_{zz} - \frac{\alpha}{\rho} \frac{\partial}{\partial z} (\eta \eta_z) - 2c_0 \beta \eta_{zzzz} = 0 ,$$

$$\eta(z, t = 0) = \eta_0 \psi(z) . \quad (9)$$

Finally it is convenient to transform to a moving frame coordinate system, defined by the parameters $t' = t$, $y = z - c_0 t$. After substitution of these variables we arrive at terms consisting of only one derivative with respect to the traveling coordinate y , except for one term having a double time derivative $\eta_{t't'}$. Neglecting this term will not change the behavior up to first order [10], as this is a 'slow' coordinate with respect to the evolution of the wave packet. Integrating the resulting expression once, we finally obtain the equation

$$\eta_{t'} + \frac{\alpha}{2\rho c_0} \eta \eta_y + \beta \eta_{y y y} = 0$$

$$\eta(y, t' = 0) = \eta_0 \psi(y) . \quad (10)$$

This is the well-known Korteweg-de Vries (KdV) equation, describing for example the formation of stable wave packets (solitons) in a narrow water channel. It can be shown that solutions of (10) also fulfill its spatial derivative, although the reverse is not necessarily true. In the next section we shall describe how to connect this equation to experiments on acoustic wave packets.

3 Physical Parameters

To make the step from (10) to an experimental configuration, the parameter range of interest for nonlinear acoustics will be discussed in this section. A general discussion of the boundary value problem of the Korteweg-de Vries equation for arbitrary $\psi(y, t = 0)$ can be found e.g. in Karpman [12]. The relevant parameter for KdV solitons turns out to be the similarity parameter σ , defined as

$$\sigma = l_0 \left(\frac{\alpha \eta_0}{2\rho c_0 \beta} \right)^{1/2} . \quad (11)$$

Here l_0 and η_0 denote the spatial width and the amplitude of the initial strain perturbation, α and β are the nonlinear and dispersive parameters, respectively. The condition for the generation of a soliton from an initial perturbation depends on the integral - or first moment - of the initial wavepacket:

$$p_0 = \int_{-\infty}^{\infty} \psi(\xi) d\xi . \quad (12)$$

Table 1. Parameters characterising the experiments of Hao and Maris compared with those of the present experimental configurations (Sec. 5 and 6). ** Values for a typical strain of 10^{-4}

Parameter	Units	Hao and Maris [2]			Sec. 5	Sec. 6
		Si [100]	MgO [100]	Al ₂ O ₃ [0001]		
l_0	nm	20			180	290
I_{pump}	J	$2 \cdot 10^{-9}$			10^{-8}	10^{-3}
w_{pump}	cm	$1.5 \cdot 10^{-3}$			$1.1 \cdot 10^{-3}$	0.15
P_{max}	W cm ⁻²	10^9			10^{10}	10^{11}
		Si [100]	MgO [100]	Al ₂ O ₃ [0001]	PbMoO ₄ [001]	
c_0	10^5 cm/s	8.48	9.05	11.23	3.63	
β	10^{-11} cm ³ s ⁻¹	1.8	1.6	3.75	13.6	
α	TPa	-0.373	-4.02	-1.83	-1.0	
σ **		4.6	12.5	4.8	21.7	35.0
N **		0.6	1.6	0.6	2.8	4.5
l_1 **	nm	13.9	4.3	13.0	21.5	21.0
$\Delta c_1/c_0$ **	10^{-4}	0.04	2.28	0.09	2.5	2.9
thickness d	mm	0.315	0.495	2.01	5.0	5.0

If $p_0 \neq 0$ then always at least one soliton will form. When, however, $p_0 = 0$, a soliton will only develop if $\sigma^2 > 7$ [12]. With increasing σ more solitons will separate from the wave packet. An approximate value for the number of solitons can be found from the inverse scattering transform for large values of σ [12]:

$$N = \left(\frac{\sigma}{\pi\sqrt{6}} \right) \int_{\psi(\xi) < 0} \sqrt{|\psi(\xi)|} d\xi . \quad (13)$$

Note that in this limiting case, the number of solitons only depends on the negative part of the initial perturbation.

In Table 1, relevant parameters both of the experiments by Hao et al. and ours, described later (see Sec. 5 and 6) are shown. Clearly one can notice important differences between both experimental configurations. The most significant difference is the initial pulse width l_0 , caused by the difference in transducer thickness. The resulting higher value of σ is partially compensated by the difference in propagation velocities and, most importantly, by the high dispersion coefficient of lead molybdate. This influences the soliton solutions of the system, both in energy content and in propagation velocity. It is well known that the shape of a Korteweg-de Vries soliton is given (in moving frame coordinates) by

$$\eta_r(y, t') = a_r \operatorname{sech}^2 l_r^{-1} (y - \Delta c_r t') , \quad (14)$$

where η_r denotes the wave function in strain of the r -th soliton developing from an initial wave packet. The soliton width, l_r , is given by

$$l_r = \sqrt{\frac{24\rho c_0\beta}{\alpha a_r}}, \quad (15)$$

and the velocity change of the soliton relative to the sound velocity, $\Delta c_r/c_0$, is given by

$$\frac{\Delta c_r}{c_0} = \frac{\alpha a_r}{6\rho c_0^2}. \quad (16)$$

For large values of σ , the strain amplitude of the r -th soliton can be approximated by [12]

$$a_r = \frac{3\eta_0}{\sigma^2} \left(1 + \sqrt{1 + 2\sigma^2/3} - 2r\right)^2. \quad (17)$$

From these expressions it follows that, for large σ , the amplitude and velocity of the solitons depend mainly on the material parameters and η_0 , and not so much on l_0 . Due to the high dispersion coefficient of lead molybdate, solitons in the current experimental configuration will not only be broader than those observed in the experiments of Hao and Maris, they will also propagate relatively faster. Theory predicts that in all four configurations of Table 1 one or more acoustic solitons will be generated at an initial strain of 10^{-4} . It should however be realized that a 290 nm wide pulse contains much more energy than one of 20 nm width of equal strain, meaning that much more pump pulse energy will be needed to achieve such a perturbation.

4 Experimental Setup

Inelastic scattering of a single-mode argon-ion laser operating at 514 nm was used to probe the local strain Fourier components in a transparent crystal (see Fig. 1). The scattered radiation, for anti-Stokes scattering shifted upward in frequency and for Stokes shifted downward, is analyzed using a quintuple-pass Fabry-Pérot interferometer (Burleigh model RC-110) and standard photon counting apparatus. For the kHz-excitation experiments of Sec. 6, additional electronic gating of the photomultiplier signal was required to cope with the small duty cycle because of the short interaction time in the scattering volume and the low pump repetition frequency. Wavevector conservation in the scattering plane ensures sensitivity of the Brillouin signal for *single* Fourier components of the wave packet, although this condition is partly relaxed due to the tight focusing ($w_B = 3.5 \mu\text{m}$) of the argon-ion laser.

The sample is a lead molybdate (PbMoO_4) single crystal of $10 \times 5 \times 6 \text{ mm}^3$ dimension, with its c -axis oriented perpendicular to the $10 \times 5 \text{ mm}^2$ interface. Lead molybdate was mainly chosen because of its extraordinary high acousto-optic coupling parameter. Further, the large acoustic dispersion parameter, as shown in Table 1, leads to a large l_{sol} and thus to a larger fraction of the acoustic power in the lower part of the spectrum, that is accessible in Brillouin scattering experiments.

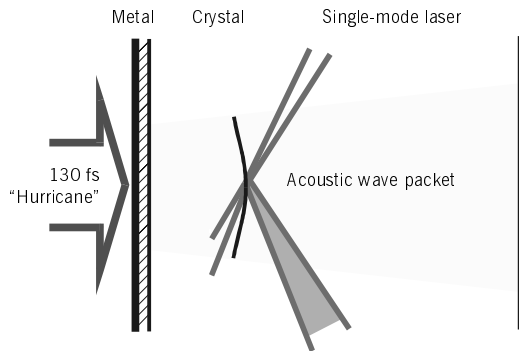


Fig. 1. Top view of the Brillouin scattering configuration in the crystal

A 500-nm gold transducer is deposited onto the $10 \times 5 \text{ mm}^2$ interface, with a 5-nm chromium interlayer for better adhesion. It is known from experiments by Wright et al. [13] that the width of an acoustic wave packet generated by femtosecond optical absorption in gold is not determined by the optical skin depth of 12 nm, but rather by the ballistic transport length of hot electrons within the electron-phonon relaxation time of about 1 ps. The tails of the acoustic wave packet will therefore be several hundred nanometers wide. The sample is contained in an optical flow cryostat at liquid helium temperatures, which is necessary to eliminate damping of the acoustic wave packet from thermal phonons. Damping of monochromatic, low-amplitude GHz phonon beams has been studied previously in lead molybdate by Damen et al. [14] and is found to correspond at liquid-helium temperatures to mean free paths much larger than the crystal dimensions.

Two different types of femtosecond pulsed laser systems have been used as an excitation source for the acoustic strain. For the diffraction experiments of Sec. 5, a mode-locked Ti:sapphire laser operating at 800 nm was used, delivering 160 femtosecond pulses of 10 nJ/pulse at 76 MHz (Coherent Mira 900). Previous experiments on mode-locked acoustic wave packets using this setup have been described in Ref. [15]. Recently, an amplified system was incorporated in the setup, delivering 130 femtosecond laser pulses of 1 mJ/pulse at 1 kHz (Spectra Physics Hurricane). Section 6 describes the first results obtained using this excitation source. A longitudinal acoustic wave packet generated in the transducer by optical absorption generally has two polarities of strain. The initial compressional strain propagates in two opposing directions, of which one is usually reflected from the interface with a lower impedance material (helium), giving an inversion of the strain polarity. The shape of the wave packet can be controlled by changing the acoustic environment of the transducer. We use two different excitation geometries, one is excitation from the helium-gold interface, the other from the crystal-gold interface.

5 Propagation and diffraction of picosecond acoustic wave packets

Before we describe our experiments we note that for a detectable strain amplitude in case of a modelocked Ti:sapphire laser, the pump beam has to be focused to a waist w_0 of about $11 \mu\text{m}$. The limited width of the corresponding acoustic beam leads to significant diffraction of the lower, GHz frequency components. Diffraction of low amplitude monochromatic phonon beams has been studied extensively in lead molybdate by Damen et al. [16] and it was shown that the waist of the strain, $w_{\text{ph}}(z)$, follows the Fraunhofer diffraction law corrected with a weak phonon (de)focusing:

$$w_{\text{ph}}(z) = w_0 \left(1 + \left(\frac{z}{z_0(1-2p)} \right)^2 \right)^{1/2}, \quad (18)$$

where p denotes the phonon focusing parameter ($p = 0.173$ for lead molybdate [17]). The corresponding theoretical divergence angle θ_{th} is given by

$$\theta_{\text{th}} = \frac{w_0}{z_0(1-2p)} = \frac{\lambda_{ac}}{(\pi w_0(1-2p))}. \quad (19)$$

We will measure the diffraction of several frequency components of an acoustic wave packet using the same method as in Ref. [17]: scans of the pump beam transverse to the acoustic beam were taken with micrometer resolution, while keeping the Brillouin scattering condition fixed. The interaction volume (overlap between acoustic beam and argon-ion laser focus) is determined by the focal volume of the argon-ion laser in the sample, which is estimated to be a cylinder of $10 \mu\text{m}^2$ by $50 \mu\text{m}$ inside the crystal.

First, the input Fourier spectrum of the wave packet was determined at room temperature, by measuring the diffracted intensity directly after the transducer at various scattering angles. We use the crystal-gold side excitation geometry in these experiments, yielding a Brillouin signal in the frequency region of interest, a factor of 50 higher than in the case of the gold-helium geometry. The observed Fourier spectrum is shown in Fig. 2. The spectral resolution in these measurements is limited to 280 MHz due the small size of the interaction volume (and the concomitant spread in diffraction angles)

At the frequencies indicated by the arrows in Fig. 2 (corresponding to maxima and minima in the spectrum), further experiments were performed at $T = 5 \text{ K}$. At each scattering configuration, the acoustic beam width was measured as function of propagation distance in the crystal for different excitation intensities. Typical traces are shown in Fig. 3 for an acoustic frequency of 7.2 GHz. At low excitation intensities, the observed beam divergence corresponds to the behavior expected for linear propagation, according to (18). For increasing pump intensities, however, anomalous behavior is observed, leading first to an increase in diffraction and, above 1.5 mJ/cm^2 , to a steep decrease of the beam divergence.

The measured diffraction angle normalized to the theoretical value of (19), versus pump intensity, is shown in Fig. 4, for the frequencies indicated in Fig. 2.

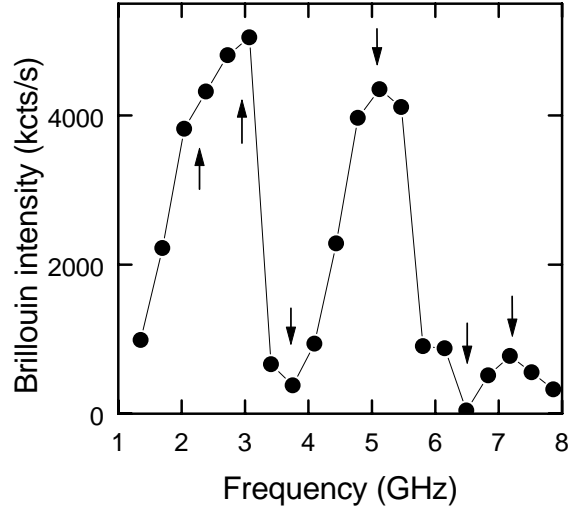


Fig. 2. Frequency spectrum of the acoustic wave packet (crystal-gold side excitation). Arrows indicate positions where diffraction experiments have been performed.

Again, the diffraction is seen to converge to the linear theory towards low pump intensities for most of the frequencies under study. Significant deviation occurs however, both in the low-intensity and the general behavior, for the minima in the spectrum of Fig 2 (at 3.8 and 6.5 GHz frequencies). These show a diffraction ratio significantly smaller than unity at all pump intensities. At the other frequencies, the normalized diffraction is seen to change for increasing excitation intensities. At intensities above 1.5 mJ/cm^2 clearly a steep decrease in diffraction is found at the maxima of the spectrum (see Fig. 2). The behavior of the 2.2 GHz component differs from that of the other frequencies by a decrease of the diffraction even at lower pump intensities. Unfortunately, our current sensitivity is not sufficient to measure below 0.1 mJ/cm^2 pump intensities and does not permit to enter the purely linear diffraction regime (of Ref. [17]). At higher pump intensities the experiment is limited by the output power of the Ti:sapphire laser.

In order to study the propagation of the complete Fourier components, the total acoustic power in the selected modes is computed as a function of z and power by integration of the Brillouin signals over each transverse scan. The resulting traces, normalized to the value measured directly after the transducer, are shown in Fig. 5. The main observation is that the acoustic power is continuously redistributed among the Fourier components constituting the wave packet. It is further remarkable that the behavior is different for the various selected Fourier components and depend on the pump intensity. For example, the acoustic power in the minima of the spectrum of Fig. 2 (at 3.8 GHz and 6.5 GHz) tends to increase during propagation, while the maxima show a significant decrease. This suggests that the spectral minima are the most sensitive to the effects of acoustic

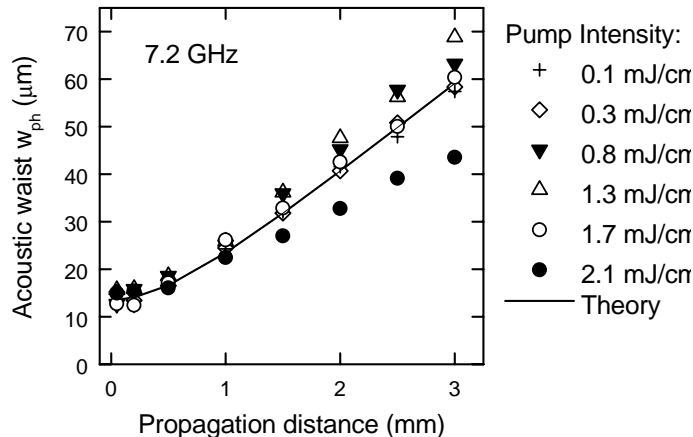


Fig. 3. Typical scans of the acoustic beam width as a function of propagation distance at $\nu = 7.2$ GHz, for several pump intensities. The solid line denotes the theoretical divergence (18) due to Fraunhofer diffraction

nonlinearity, which might be a clue in understanding their anomalous diffraction at low pump intensities in Fig. 4. All our measurements suggest that we are dealing with a regime in which nonlinearity plays an important role and significantly influences the diffraction of the wave packet. Attempts have been made to describe the observations of Fig. 5 by simulations based on the one-dimensional wave equation of section 2 (results not presented in this article). Although exact fits could not be obtained, the qualitative behavior of the different parts of the spectrum could be reproduced within reasonable agreement. These simulations, for the relevant parameters (see Table 1), show significant self-steepening of the wave packet, combined with the onset of dispersion, for strains of the order of 10^{-5} . Work is in progress to include diffraction into the wave equation in order to explain the nonlinear diffraction of the wave packet in this regime.

Acoustic beam propagation in the nonlinear regime has been studied extensively in the absence of dispersion, giving rise to the formation of shock waves (see e.g. Ref. [10]). It was shown that compressional shock waves tend to defocus while rarefaction shock waves will focus. As we are dealing with bipolar wave packets in which only the compressional wave is stable to dispersion (as we learned from the simulations mentioned above), an increase in diffraction with excitation power would be expected from this theory, which clearly is contradictory to our observations at high pump intensities.

Another mechanism which could lead to a decrease in diffraction is the refraction of the acoustic beam due to a radial thermal gradient in the crystal. It is known that an increase in lattice temperature in the center of the beam leads to refraction of an acoustic wave which has a focusing effect [10]. This mechanism however would equally work for all Fourier components, and would strongly depend on the amount of energy deposited in the system and thus on

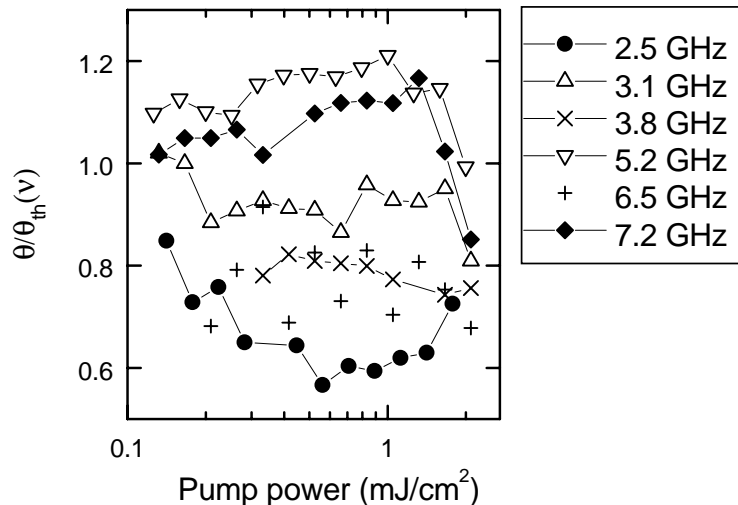


Fig. 4. Divergence angle of the different frequency components indicated in Fig. 2 normalized to the theoretical values of (19), as a function of pump intensity.

the pump intensity. Further, at low temperatures the phonon mean free paths are so long that significant localized heating of the crystal is absent.

The problem of propagation of a cylindrical symmetric beam and the formation of solitons in a quadratic nonlinear medium *with* dispersion has become a lively subject to study very recently in the case of optical fields [18], [19], [20], [21]. The mechanism leading in Ref. [19] to stable spatial solutions is the continuous up- and down-conversion between coupled modes, which in combination of either normal or anomalous dispersion leads to a wave-front reshaping which compensates the positive curvature due to diffraction. In the optical case of second harmonic generation generally only three modes are present, whereas we are dealing with a large number of modes of the acoustic wave packet (note that one can see a single cycle wave packet as a very broad spectrum of harmonics). It seems however, that the physical principles underlying the coupling between these modes are equal, so similar behavior might be expected. To which extent these mechanisms are indeed present in our current experiment will be a subject of future study.

6 One-dimensional propagation experiments

Although the physics of three-dimensional wave packet propagation is an extremely interesting subject of studies, one would certainly also want to be able to perform a more one-dimensional propagation experiment. It is not possible to make a large-area acoustic field which is intense enough for nonlinear acous-

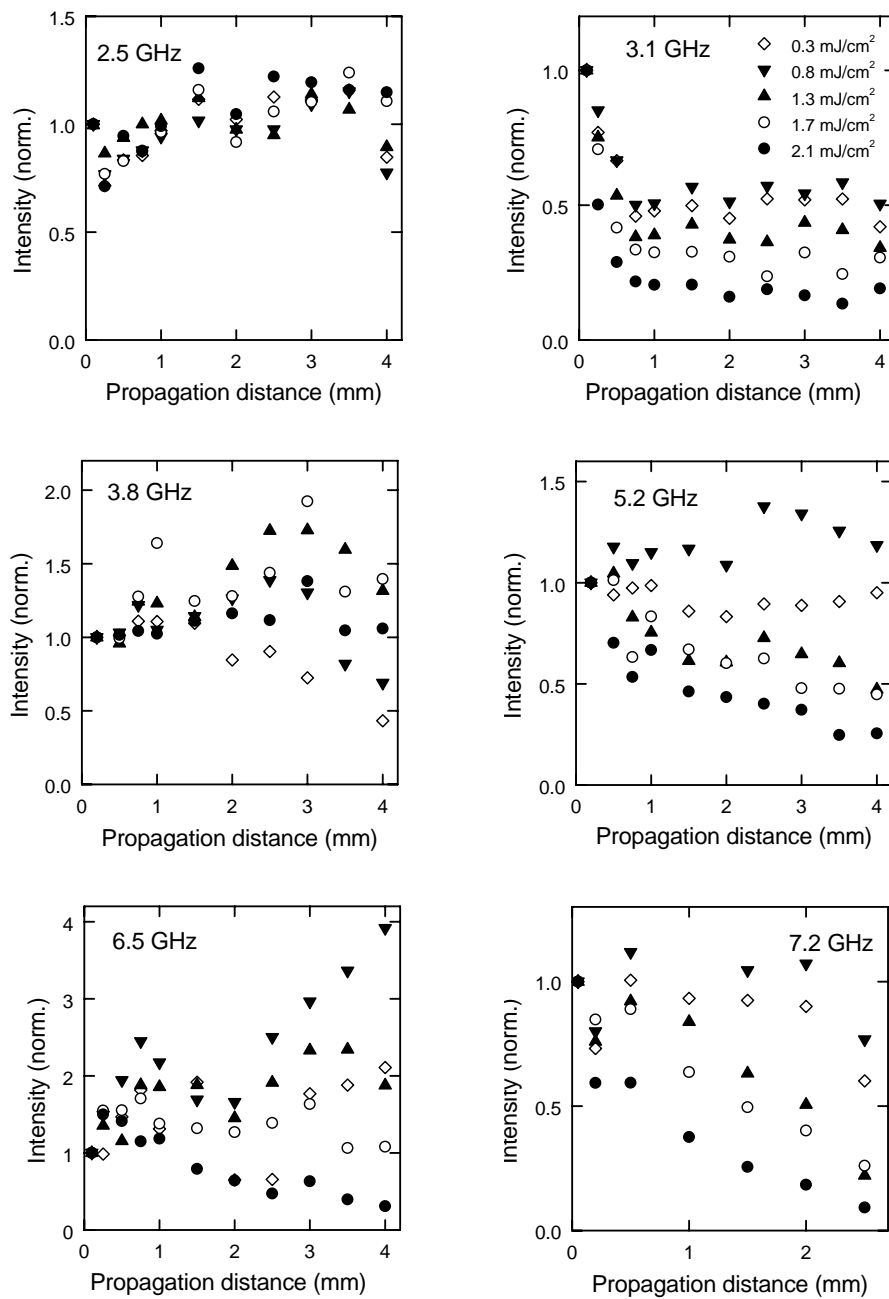


Fig. 5. Propagation of the frequency components as indicated in Fig. 2 into the lead molybdate crystal, for different pump intensities.

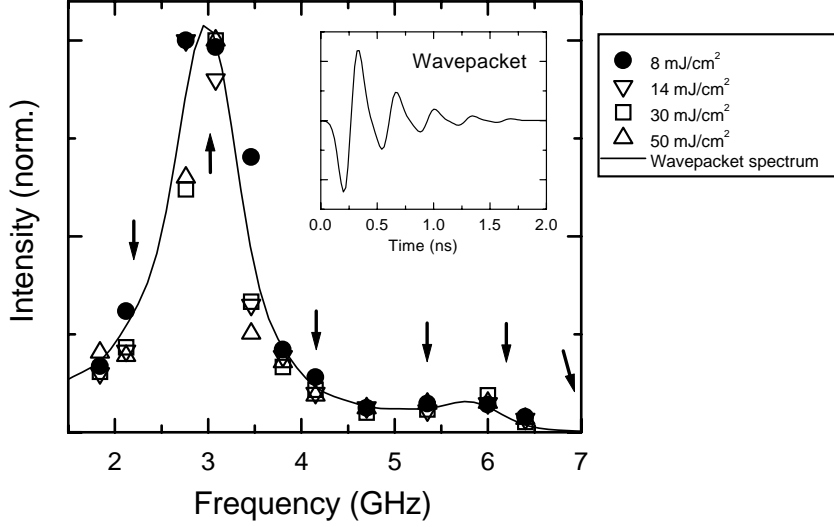


Fig. 6. Frequency spectrum of the acoustic wave packet, obtained using a 1kHz, high intensity pump laser (helium-gold side excitation). Inset: acoustic wave packet profile obtained from fitting the power spectrum.

tics to play a role using a mode-locked Ti:sapphire laser. Therefore, experiments have been initiated employing an amplified ultrafast laser system as described in section 4. The 1 mJ/pulse output of this laser is, without attenuation, weakly focused onto the metal transducer by a lens of $f = 1.6$ m focal distance. The local optical intensity at the transducer is varied by changing the distance between lens and sample (always kept smaller than f), in combination with a 1.5 mm pinhole near the sample to maintain a constant illuminated area. It was observed that even transparent materials like quartz show irreversible damage when exposed to a peak power density above 10^{13} W/cm². The damage threshold for a gold film at room temperature was determined to be an order of magnitude lower. The minimal optical waist at the gold film was therefore limited to 1.5 mm. At these high pump intensities significant nonlinear optical effects could be observed in the lead molybdate crystal, therefore experiments were performed in the helium-gold side excitation geometry, preventing the light to enter the crystal.

The incident acoustic frequency spectrum was obtained at $T = 5$ K, which is shown in Fig. 6. We observe a peak at an acoustic frequency of 3 GHz, which corresponds to the gold film thickness of 500 nm. The inset shows the acoustic wave packet that fits the measured power spectrum. The obtained fitting parameters are: $l_0 = 290$ nm for the width of the tails of the packet and $r = 0.4$ for the reflectivity between gold and lead molybdate. At the frequencies indicated by the arrows in Fig. 6, traces were made at $T = 5$ K as a function of propagation distance into the crystal for different pump intensities. The results of these

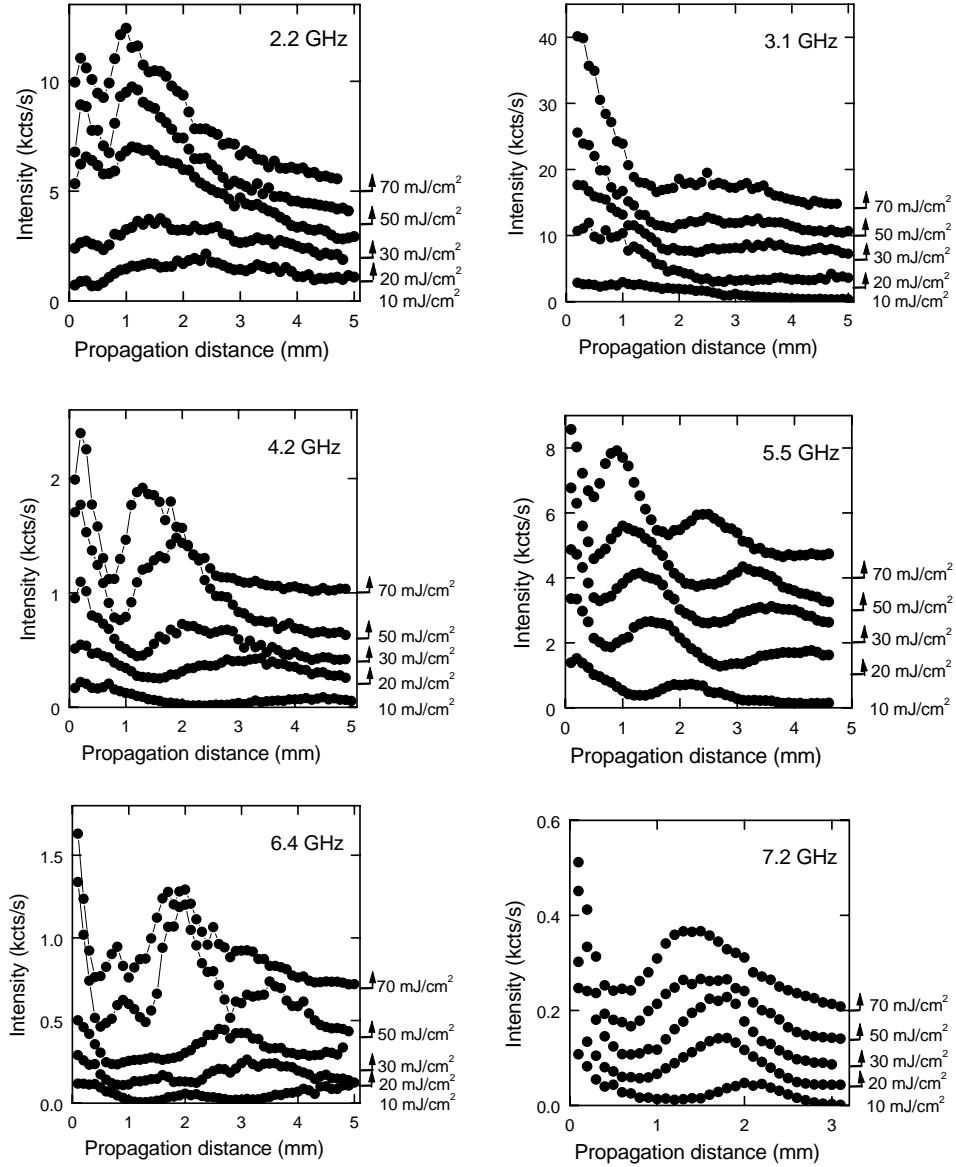


Fig. 7. Scans of the acoustic power of the frequency components as indicated in Fig. 6 as a function of propagation distance into the lead molybdate crystal, for different pump intensities. Arrows on the right indicate vertical offsets for the individual traces.

experiments are shown in Fig. 7. One immediately sees that the propagation is strongly anomalous at all frequencies under study, indicating the presence of nonlinear acoustical effects. One is able to discern oscillations in the propagation at frequencies above 4 GHz, which indicate that acoustic power is redistributed over the spectrum in a coherent manner. The initial spectral peak at 3.1 GHz is decreasing rapidly as the wave packet propagates into the crystal, until the intensity is about as high as at the other frequencies in the spectrum. This is also a strong evidence for the redistribution of acoustic power over the spectrum.

Numerical simulations of the one-dimensional KdV equation, with an initial wave packet as found from Fig. 6 yield a propagation of the Fourier components in qualitative agreement with our experimental findings. Typical evolution of the spectral components over the propagation distance is shown in Fig. 8. The spectral maximum at 3.1 GHz decreases within 1 mm propagation distance, while oscillations appear at significantly higher frequencies than generated in the initial wave packet, and start shifting through the spectrum. In these simulations, multiple solitons can be observed at a strain of the order of 10^{-4} , which is in agreement with the estimate of Table 1. The similarity between simulations and experiments strongly suggests that we are indeed in a regime in which wave packet propagation is dominated by nonlinear and dispersive terms. To which extent dispersion plays a role to form stable packets, i.e. to an acoustic soliton, can however not yet be determined with certainty. Better quantitative agreement between simulations and experiments is needed to determine whether the wave propagation can be described effectively by the one-dimensional KdV equation. Further experiments, also on different crystalline materials, will have to shed more light on these questions in the near future.

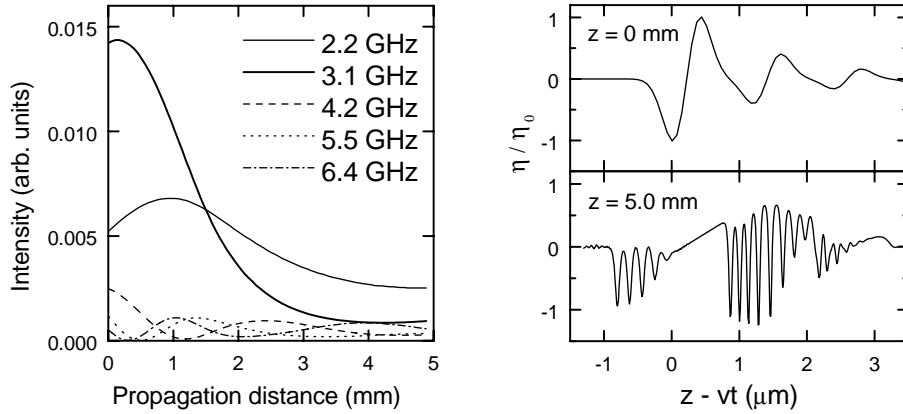


Fig. 8. (right) Propagation of the acoustic wave packet obtained from Fig. 6 over a distance of 5 mm through the crystal. (left) Evolution of individual spectral components as a function of propagation distance.

7 Conclusion

The propagation of an 80 picosecond acoustic wave packet has been studied in a lead molybdate single crystal. Diffraction of individual frequency components has been shown to converge to the linear theory of Fraunhofer diffraction combined with phonon focusing at low excitation intensities, for all frequencies except those at the minima of the spectrum. At higher pump intensities however, anomalous diffraction is observed at all frequencies, its characteristics changing over the spectrum in a nontrivial manner. This anomalous behavior has not yet been explained quantitatively, although we suspect that the explanation might be found in the coupling between acoustic frequencies in combination with dispersion. This mechanism might provide the necessary reshaping of the wave front which can counterbalance diffraction, as has been observed for light pulses in second harmonic generation in quadratically nonlinear optical systems. Further experiments, extending the dynamic range in both the high- and low excitation intensity regimes, will be performed in the near future.

Results on one-dimensional propagation at high peak intensities show strongly nonlinear propagation of frequency components of the wave packet. Oscillations appear which can be explained by a coherent redistribution of acoustic power over the spectrum. Comparison with the theory of nonlinear wave propagation shows that similar features are an indication of self steepening and even soliton formation. This strongly suggests that we are in a regime of strong nonlinear behavior, which is remarkable considering the relatively low frequency range under studies. It is however consistent with the expected parameters for nonlinearity and dispersion in the lead molybdate system. Future experiments, especially in combination with time domain spectroscopy, will certainly provide more insight in the nature of wave packet evolution at these experimental conditions.

The authors would like to thank C.R. de Kok, P. Jurrius and F.J.M. Wollenberg for their technical support. This work was supported by the Netherlands Foundation “Fundamenteel Onderzoek der Materie (FOM)” and the “Nederlandse Organisatie voor Wetenschappelijk Onderzoek (NWO).”

References

1. A.M. Samsonov, G.V. Dreiden, A.V. Porubov, and I.V. Semenova. Longitudinal-strain soliton focussing in a narrowing nonlinearly elastic rod. *Phys. Rev. B*, 57(10):5778, 1998.
2. H.-Y. Hao and H.J. Maris. Experiments with acoustic solitons in crystalline solids. *Phys. Rev. B*, 64(6):4302, 2001.
3. H.-Y. Hao and H.J. Maris. Study of phonon dispersion in silicon and germanium at long wavelengths using picosecond ultrasonics. *Phys. Rev. Lett.*, 84(24):5556, 2000.
4. M.A. Breazale and J. Ford. Ultrasonic studies of the nonlinear behavior of solids. *J. Appl. Phys*, 36(11):3486, 1965.
5. O.B. Wright and K. Kawashima. Coherent phonon detection from ultrafast surface vibration. *Phys. Rev. Lett.*, 69(11):1668, 1992.

6. D.H. Hurley and O.B. Wright. Detection of ultrafast phenomena by use of a modified Sacnac interferometer. *Opt. Lett.*, 24(18):1305, 1999.
7. B.A. Auld. *Acoustic fields and waves in solids*, volume 1. Robert E. Krieger Publishing Company, 2nd edition, 1990.
8. R.S. Rivlin. Large elastic deformations of isotropic materials. *Phil. Trans. A*, 240:459, 509, 1948.
9. A. Seeger and O. Buck. Die experimentelle Ermittlung der elastischen Konstanten höherer Ordnung. *Z. Naturforsch.*, 15a:1056, 1960.
10. K. Naugolnykh and L. Ostrovsky. *Nonlinear wave processes in acoustics*. Cambridge Texts in Applied Mathematics. Cambridge University Press, 1st edition, 1998.
11. T. Bateman, W.P. Mason, and H.J. McSkimin. Third-order elastic moduli of germanium. *J. Appl. Phys.*, 32(5), 1961.
12. V.I. Karpman. *Non-linear waves in dispersive media*. Pergamon Press, 1st edition, 1975.
13. O.B. Wright. Ultrafast nonequilibrium stress generation in gold and silver. *Phys. Rev. B*, 49(14):9985, 1994.
14. E.P.N. Damen, A.F.M. Arts, and H.W. de Wijn. Experimental verification of Herring's theory of anharmonic phonon relaxation: TeO₂. *Phys. Rev. B*, 59(1):349, 1999.
15. O.L. Muskens and J.I. Dijkhuis. Propagation of ultrashort acoustic wave packets in PbMoO₄ studied by Brillouin spectroscopy. *Physica B*, (To be published).
16. E.P.N. Damen, D.J. Dieleman, A.F.M. Arts, and H.W. de Wijn. Generation and propagation of coherent phonon beams. *Phys. Rev. B*, 64(17):4303, 2001.
17. E.P.N. Damen, A.F.M. Arts, and H.W. de Wijn. High-frequency monochromatic acoustic waves generated by laser-induced thermomodulation. *Phys. Rev. Lett.*, 75(21):4249, 1995.
18. Ll. Torner, D. Mazilu, and D. Mihalache. Walking solitons in quadratic nonlinear media. *Phys. Rev. Lett.*, 77(12):2455, 1996.
19. W.E. Torruellas, Z. Wang, D.J. Hagan, E.W. VanStryland, G.I. Stegeman, Ll. Torner, and C.R. Menyuk. Observation of two-dimensional spatial solitary waves in a quadratic medium. *Phys. Rev. Lett.*, 74(25):5036, 1995.
20. X. Liu, K. Beckwitt, and F. Wise. Two-dimensional spatiotemporal solitons in quadratic media. *Phys. Rev. E*, 62(1):1328, 2000.
21. D. Mihalache, D. Mazilu, L.-C. Crasovan, Ll. Torner, B. Malomed, and F. Lederer. Three-dimensional walking spatiotemporal solitons in quadratic media. *Phys. Rev. E*, 62(5):7340, 2000.